Spectroscopic and Kinetic Investigation of Methylene Amidogen by Cavity Ring-Down Spectroscopy

Boris Nizamov[†] and Paul J. Dagdigian*

Department of Chemistry, The Johns Hopkins University, Baltimore, Maryland 21218-2685

Received: October 7, 2002; In Final Form: January 24, 2003

Cavity ring-down spectroscopy (CRDS) has been used to study room-temperature chemical reactions of the methylene amidogen radical (H_2CN). The radical was prepared by 193 nm photolysis of formaldoxime, $H_2CNOH \rightarrow H_2CN + OH$. CRDS signals from both H_2CN and OH [$A - X$ (1,0) band] were observed in the wavelength region 278−288 nm. By comparison of the strengths of the OH and H_2CN signals, the oscillator strength of H_2CN electronic transition in the 279−288 nm wavelength region was measured to be 4.5×10^{-4}. To correct for the loss of the OH signal due to reactions of OH, the room-temperature rate constant for the reaction of OH with formaldoxime was measured, $k(H_2CNOH + OH) = (1.5 \pm 0.4) \times 10^{-12}$ cm^3 molecule^{-1} s^{-1}. Reaction of H_2CN with a number of stable molecules [O_2, C_2H_4, CO, CH_4, H_2] could not be observed, and an upper limit to the reaction rate constants, $< 1 \times 10^{-15}$ cm^3 molecule^{-1} s^{-1}, was derived. Self-recombination was the main removal process for the H_2CN radical under the conditions of the experiment, with the rate constant $k(H_2CN + H_2CN) = (7.7 \pm 2.5) \times 10^{-12}$ cm^3 molecule^{-1} s^{-1}. At high photolysis laser energies, for which the H_2CNOH fractional dissociation was high, it was possible to study the reaction of H_2CN with OH. A value of the rate constant for the $OH + H_2CN$ reaction, $k(OH + H_2CN) = 6 \times 10^{-12}$ cm^3 molecule^{-1} s^{-1}, was derived.

1. Introduction

The methylene amidogen radical (H_2CN) is an important intermediate in a number of chemical processes.[1] It is an intermediate in the thermal decomposition of nitramine propellants, such as HMX and RDX.[2−4] This radical is also believed to play a role in the combustion chemistry of hydrocarbon flames containing nitrogen (through the $N + CH_3$ reaction[5,6]), in the reburning of NO (through the $CH_3 + NO$ reaction[7]), and in the chemistry of the atmosphere of Titan and in interstellar clouds.[1,8]

The H_2CN radical has been investigated using a variety of experimental methods, including ESR spectroscopy,[1,9] flash photolysis,[10,11] IR and UV absorption in cryogenic matrixes,[12] photoionization studies,[13] and H-atom photofragment translational energy spectroscopy.[14] The UV absorption bands of H_2CN near 280 nm were first observed some years ago in the flash photolysis of formaldazine ($H_2CN-NCH_2$) and formaldoxime (H_2CNOH) by Horne and Norrish[11,15] and Ogilvie and Horne.[10] The 193 nm photodissociation of formaldazine has been studied by molecular beam photofragment translational spectroscopy with mass spectrometric detection of the H_2CN fragments.[16] The UV absorption spectrum of H_2CN trapped in solid argon was later reported by Jacox.[17] Dagdigian et al.[18] attempted to detect H_2CN and its methylated analogues by laser fluorescence excitation of the bands near 280 nm with 193 nm photolytic preparation from various precursors (mainly the oximes). While the OH fragment from the photodissociation of the oximes was readily detected, they concluded that the fluorescence quantum yield for H_2CN was negligible and that the excited state decays by predissociation.

In a molecular beam study, Davis and co-workers[14] recently observed the bands of the H_2CN radical near 280 nm through Rydberg atom detection of the H atom fragment from predissociation of electronically excited H_2CN. The H_2CN radical was prepared in a molecular beam by pyrolysis of formaldazine at the beam orifice. They also measured the kinetic energy distribution of the H atom fragments and thus estimated the internal excitation of the HCN cofragment, which was found to contain a wide distribution of internal excitation energies. This work showed that H_2CN could be detected by laser-based methods; however, the particular scheme employed is not particularly amenable to kinetic and spectroscopic studies.

In earlier work, Steif and co-workers[1,5,6] employed electron-impact ionization detection to study the kinetics in flow-tube experiments of some reactions involving the H_2CN radical. They prepared H_2CN by the reaction of N atoms with methane, and H_2CN was detected by a mass spectrometer, with electron-impact ionization, through a sampling port. There were some problems associated with this method. In particular, vibrationally excited N_2 was also present in these experiments and interfered with the detection of H_2CN since both species have the same mass-to-charge ratio ($m/e = 28$). This interference could be alleviated by using very low electron energies (~12 eV), but at the expense of a very poor signal-to-noise ratio.

The use of deuterated reagent to generate D_2CN allowed higher electron energies since the background at $m/e = 30$ was much less. This group studied the reactions of N and H atoms with methylene amidogen,[19] as well as the formation of H_2CN in the $N + CH_3$ reaction.[5,6] The determination of the rate constant for the $N + H_2CN$ reaction was complicated by the fact that N atoms are involved in both the formation and destruction of H_2CN and that the rates of these processes are comparable. As an alternative ionization method to electron impact, photoionization can be applied to the detection[13] of H_2-

* Corresponding author.
[†] Present address: Department of Chemistry, The University of California, Berkeley, CA 94720.

10.1021/jp022197i CCC: $25.00
Published on Web 03/12/2003

CN and was used by Davis and co-workers at a wavelength of 118 nm to detect this species in a molecular beam.[14]

The aim of the present work was to explore the use of cavity ring-down spectroscopy (CRDS) to study the spectroscopy and chemistry of H_2CN. The CRDS technique has a good spatial resolution and sensitivity and has been used extensively to study reactive intermediates in flames and other environments.[20−23] This and the unsuitability of the convenient laser-induced fluorescence (LIF) probe for H_2CN makes CRDS particularly appropriate for kinetic studies of H_2CN chemistry.

There have been several theoretical studies on the ground and excited electronic states of H_2CN and its possible role as an intermediate in the $H + HCN \rightarrow H_2 + CN$ reaction. The ground electronic state of the H_2CN radical has $^2B_2$ symmetry.[1] Adams et al.[24] calculated structural parameters for the ground electronic state and vertical excitation energies to four excited states. These calculations suggested that the lowest-energy absorption feature at 285 nm is due to an electronically forbidden but vibronically allowed transition to a $^2B_1$ state, while the stronger transition at 280.8 nm was assigned as a symmetry-allowed $^2A_1 \leftarrow {}^2B_2$ transition. Davis and co-workers[14] have measured the H atom recoil anisotropy parameter β for the H atom fragment from the dissociation of electronically excited H_2CN and found that this parameter is slightly negative [$\beta = -0.10 \pm 0.03$]. Interpretation of this value provides some information on the symmetry of the excited state. This value of β rules out an excited-state $^2A_1$ symmetry but is consistent with a vibronically allowed transition to a $^2B_1$ excited state.

In a quantum chemical study, So[25] suggested that the first electronically excited state ($^2B_1$) has a nonplanar $^2A'$ equilibrium geometry. Brinkmann et al.[26] recently carried out a coupled-cluster study to determine geometries and harmonic vibrational frequencies for the ground and low-lying excited electronic states of H_2CN. Their computed harmonic vibrational frequencies are in reasonable agreement with those reported by Jacox in an Ar matrix study.[17] Brinkmann et al. report that the lowest $^2B_1$ and $^2A_1$ excited states (labeled as $\tilde{A}\ ^2B_1$ and $\tilde{C}\ ^2A_1$ by these workers, respectively) have planar equilibrium geometries as in the ground state, while the 2^2B_1 state (labeled as $\tilde{B}\ ^2A'$), and not the 1^2B_1 state as proposed by So,[25] is nonplanar.

The H_2CN radical is also a possible intermediate in the $H + HCN \rightarrow H_2 + CN$ reaction.[27] However, it appears that a ridge separates the H_2CN well from the abstraction pathway on the potential energy surface.[28]

In the present study, we have employed the transition at 280 nm for a kinetic and spectroscopic study of H_2CN by the CRDS technique. Formaldoxime was chosen as a photolytic precursor for H_2CH for several reasons. It does not have significant absorption near 280 nm[15] and hence will not interfere with the H_2CN measurements. The other fragment from formaldoxime photolysis is the hydroxyl radical, which has a spectroscopic transition [$A - X$ (1,0) band] in the same region where H_2CN absorbs. Comparison of the OH and H_2CN signals will allow the determination of the absorption strength of the H_2CN transition. Reactions of H_2CN with a number of stable molecules [O_2, C_2H_4, CO, CH_4, H_2] were investigated, and only upper bounds to the rate constants could be determined. A rate constant for the $OH + H_2CN$ reaction is also reported in this paper.

2. Experimental Section

Experiments were carried out in a flow cell consisting of the central parallelepiped ($2.0 \times 3.0 \times 20$ cm) with two rectangular photolysis side windows (1.2×13.5 cm) and two baffle arms. The cavity ring-down mirrors [Rocky Mountain Instrument Co., 99% reflectivity at 282 nm] were mounted on the end of the baffle arms, and the distance between the mirrors was 50 cm. Baffles were installed to decrease contamination of the mirrors by dust and to block the fluorescence signal excited by the excimer laser, which could interfere with the CRDS signal at short delay times.

Photolysis of formaldoxime vapor at 193 nm was used to produce H_2CN and OH radicals. The photolysis source was a Lambda Physik Compex 102 excimer laser. Typical pulse energies of the excimer laser inside the vacuum chamber were 20−100 mJ. The excimer laser beam was directed perpendicular to the axis of the CRDS resonant cavity, and two cylindrical lenses were used to shape the excimer laser beam. One lens was used to expand the beam along the cavity axis, and the second lens was used to compress the beam along the direction perpendicular to the cavity axis. After the two lenses, the excimer laser beam profile was rectangular with 0.2×7.0 cm dimensions on the axis of the cavity. The delay between the excimer and the dye laser was controlled by a digital delay generator (Stanford Research Systems DG535).

Formaldoxime polymer was prepared by the procedure given by Scholl,[29] involving the reaction of formaldehyde with hydroxylamine. Water was removed from a paste-like product by pumping through a liquid nitrogen trap. Formaldoxime vapor was introduced into the vacuum chamber using two different procedures. When high pressures of the buffer gas were required, the buffer gas was flowed through a glass tube filled with the solid polymeric formaldoxime. Glass wool was used to prevent formaldoxime dust from going inside the chamber. When pure formaldoxime vapor was used, formaldoxime was introduced from a test tube, sealed to a vacuum chamber using an O-ring. In both cases formaldoxime polymer was heated to temperatures of less than 55 °C to increase its vapor pressure.

Tunable UV radiation in the 278−288 nm range was generated by frequency doubling the output of a home-built grazing-incidence dye laser, pumped by a Nd:YAG laser (Continuum NY-81C) operated at 10 Hz. The second harmonic was separated from the fundamental dye laser radiation using a UG-5 (Schott) color filter. The temporal width of a laser pulse was 8 ns, and the spectral bandwidth of the doubled output was 0.4 cm^{-1}. High-resolution spectral scans (fwhm 0.08 cm^{-1}) were taken with an intracavity etalon narrowed dye laser (Lambda Physik FL3002E). Two apertures were used to used to control the size of the UV laser beam in order to reduce the number of transverse modes excited in the cavity. One aperture reduced the beam diameter, and the second was used to remove diffraction rings. The UV laser beam was injected into the resonant cavity through one of the mirrors, and the diameter of beam in the cell was 0.05 cm. The CRD signal was detected through the rear mirror with a Hamamatsu R928 photomultiplier tube (PMT). A diffuser and color filters were placed in front of the PMT. The diffuser was used to minimize possible problems resulting from the nonuniformity of the detector area response and cavity alignment. Color filters were used to suppress stray light from the dye laser.

The CRD signal was digitized using a LeCroy 9360 digital oscilloscope. The signal from each laser shot was transferred to a computer, and a weighted least-squares fit procedure was used to calculate the photon decay rate constant. The typical decay time constant τ for the empty cavity was 150 ns. At a given wavelength single-shot decay rate constants were averaged over a preset number of shots (10−30) with the excimer laser on and excimer laser off, then the dye laser wavelength was stepped to the next wavelength point. Ring-down lifetimes could

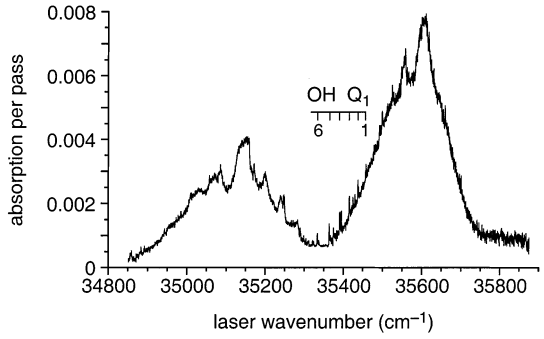

Figure 1. Cavity ring-down (CRD) absorption spectrum of photolyzed formaldoxime (500 mTorr in 5 Torr Ar). The spectrum was collected at 30 μs delay between the photolysis and detection laser pulses. Under these conditions, the methylene amidogen and OH radicals are thermally equilibrated to room temperature. The broad features are due to methylene amidogen; also observable are lines of the OH $A - X$ (1,0) band. The OH lines in the Q_1 branch are identified.

be determined to an accuracy of 1%. The signal due to the transient species produced by the photolysis laser was obtained by subtracting the decay constant with the excimer laser off from that with the excimer laser on. Hence, H_2CN was generated in the cell at a 5 Hz repetition rate. The gas in the photolysis volume was replenished on each shot, as we observed no buildup of the H_2CN concentration on successive laser pulses after the photolysis laser was turned on.

For laser-induced fluorescence (LIF) experiments, the fluorescence signal was detected by a Hamamatsu R666S photomultiplier (PMT) in a direction perpendicular both to the cavity axis and the photolysis beam direction. About 5% of the dye laser output was split using a quartz flat and directed into the vacuum chamber through one of the photolysis windows. Using a right angle prism placed inside the chamber, the LIF laser beam was directed at ~20 degrees relative to the cavity axis in a plane of the excimer laser beam. This was necessary to ensure that the LIF beam samples the same concentrations as the CRDS beam. A mask was used to limit the field of view of the PMT to the region near the cavity axis. The frequency-doubled dye laser was tuned to the OH $A - X$ (1,0) band, and an interference filter was used to observe fluorescence in the OH $A - X$ (1,1) band. The band-pass of the filter was wide enough to collect essentially all fluorescence in the (1,1) band. The signal from the PMT was directed to a gated integrator (Stanford Research Systems SR250) or digital oscilloscope (LeCroy 9360) and then transferred to a computer for processing. The first 50 ns of the waveform were used to measure the OH LIF signal to avoid problems associated with the quenching of upper-state fluorescence.

3. Results

3.1. Spectrum of the Methylene Amidogen Radical. Figure 1 presents a cavity ring-down (CRD) absorption spectrum of photolyzed formaldoxime, with many collisions between the photolysis and the CRD laser pulse (argon buffer gas at 5 Torr and a delay of 30 μs). The CRD signals are plotted as absorption per pass due to the photolytically produced species. Clearly visible in the spectrum are broad features attributable to the H_2CN radical, as described below. In addition, sharp lines of the OH $A - X$ (1,0) band[30] are weakly observed. In Figure 1, we have marked the lines in the Q_1 branch of this band.

The features assigned to H_2CN resemble closely the previously reported spectra of this radical.[10,14] The spectrum displayed in Figure 1 has two broad features, as does the absorption spectrum obtained in a flash photolysis study by Ogilvie and Horne.[10] In fact, our spectrum and theirs are essentially identical in shape, except for minor differences due to differences in the respective spectral resolutions. It should be noted that their sample had many more collisions to equilibrate (nitrogen buffer gas at 240 Torr and a delay of 200 μs) than in our experiment. This strongly suggests that our sample is thermally equilibrated. The spacing between the maxima of these two features is 558 cm^{-1}.

In their study with a pyrolysis molecular beam source, Davis and co-workers[14] observed the two broad features displayed in Figure 1a, as well as a third, weaker feature to slightly lower wavenumbers. Since their source may be expected to produce radicals with considerable vibrational excitation, this third feature may be a hot band.[14] Ogilvie and Horne do observe a very weak feature at approximately the same wavenumber.[10] It should be noted that the lowest vibrational frequency of H_2CN is 913 cm^{-1}.[17]

The two broad features in the thermalized H_2CN CRD spectrum displayed in Figure 1 do possess some additional structure. Somewhat less resolved, similar structure was evident in the flash photolysis spectrum reported by Ogilvie and Horne.[10] The spectrum obtained by Davis and co-workers[14] showed less structure, presumably because of the higher internal excitation of the H_2CN radicals prepared in the pyrolysis source.

As discussed in the Introduction, a definitive assignment of the excited electronically excited state(s) involved in the UV absorption spectrum of H_2CN has not been forthcoming. Spectra such as that presented in Figure 1 and wider scans reported elsewhere[10] do not show obvious vibronic structure. Davis and co-workers[14] have presented strong arguments for the assignment of these bands to the vibronically induced $\tilde{A}\ ^2B_1 \leftarrow \tilde{X}\ ^2B_2$ transition. This implies that the transition involves excitation to A_2 vibronic levels [to excited-state vibrational levels of b_2 symmetry, i.e., ν_5 (3103 cm^{-1}) or ν_6 (913 cm^{-1})[17]]. Alternatively or in addition, a transition to the nonplanar $\tilde{B}\ ^2A'$ state[26] could be involved.

To explore these possibilities further, we have compared our spectrum with rigid-rotor simulations of a vibrational band. The rotational constants were computed on the basis of the equilibrium geometries of the ground and excited states as calculated by Brinkmann et al.[26] A vibronically induced transition to the $\tilde{A}\ ^2B_1$ state would follow type-C rotational selection rules.[31] From the observation of Davis and co-workers[14] that the H atom photofragments recoil with an anisotropic angular distribution, it can be assumed that the excited-state lifetime τ_{exc} is not significantly larger than the rotational period. Our assumed Lorentzian width of 10 cm^{-1} fwhm corresponds to a value of 0.5 ps for τ_{exc}, which is comparable to the estimated rotational period for the most probable rotational level J of thermalized H_2CN.

Figure 2 presents a simulation of a type-C band contour for a room-temperature sample. The band contour displays a central peak, with weaker peaks on the high wavenumber side of the contour. The latter peaks are due to the K structure of the band. This computed contour bears some resemblance to the lower-wavenumber broad feature in our experimental CRD spectrum of thermalized H_2CN [Figure 1]. The experimental spectrum does show some subsidiary maxima on the high wavenumber side of this feature, although their spacing is greater than in the simulated spectrum displayed in Figure 2.

The overall widths of both features in the experimental spectrum are greater than the simulation in Figure 2 of a single vibronic band. This suggests that there could be several vibronic transitions underlying each of these features. Vibronic assignments in the spectrum of H_2CN is still not possible. Unfortu-

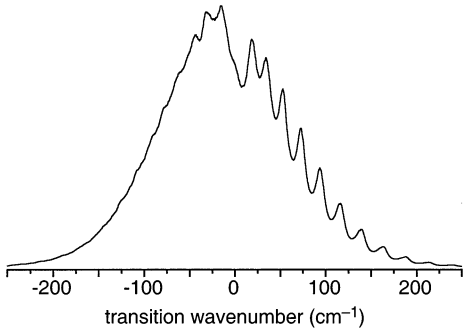

Figure 2. Simulated band contour for a vibronically induced H_2CN $\tilde{A}\ ^2B_1 \leftarrow \tilde{X}\ ^2B_2$ transition (type-C transition). The upper- and lower-state rotational constants were computed from the equilibrium geometries obtained by Brinkmann et al. (ref 26) in their quantum chemical study of this radical. A rotational temperature of 300 K and a Lorentzian fwhm of 10 cm^{-1} were assumed. The band origin wavenumber was set to zero.

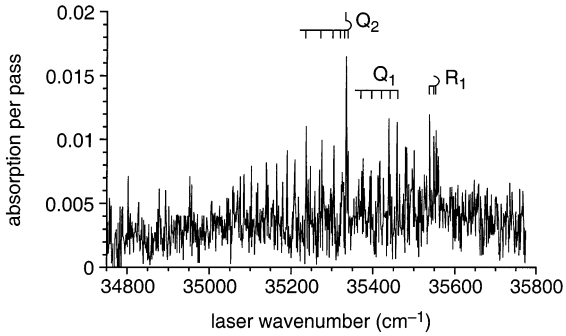

Figure 3. CRD spectrum of photolyzed formaldoxime (500 mTorr in 5 Torr Ar), collected at 500 ns delay. The OH lines in several branches of the OH $A - X$ (1,0) band are identified.

nately, complete information on the expected vibrational frequencies in the electronically excited states is not available from theoretical studies. The most complete computational study of H_2CN, i.e., the work of Brinkmann et al. reported only the harmonic frequencies for the totally symmetric vibrational modes in the excited states.

Figure 3 presents a CRD spectrum obtained with a short delay between the photolysis and CRD laser pulses. The absorption due to the H_2CN radical is much less structured and spreads over a larger wavenumber range than in the spectrum of the thermalized sample displayed in Figure 1. This implies that 193 nm photolysis of formaldoxime yields H_2CN with considerable internal excitation. It should be pointed out that the spectra in both Figures 1 and 3 were recorded by taking the differences of the CRD decay rates with the photolysis laser on vs off, and hence the unstructured absorption in Figure 3 can be assigned to photolytically produced H_2CN. As the number of collisions between the photolysis and CRD probes lasers increases, the spectrum evolves into the appearance of the spectrum of a thermalized sample, shown in Figure 1.

Even though the wavenumber sampling interval for the spectrum shown in Figure 3 was too large to record accurate intensities of the OH rotational lines, it is obvious that the OH signal at long delays is much smaller relative to the H_2CH signal than at short delays. The intensities of the OH rotational lines indicate that the rotational excitation of the OH fragment is higher than in a room-temperature Boltzmann distribution. This is consistent with the previous measurements of the OH internal state distribution by Dagdigian et al. through LIF detection.[18]

The comparison of H_2CN and OH CRD signals is made more quantitatively in Section 3.4, and a higher-resolution CRD scan

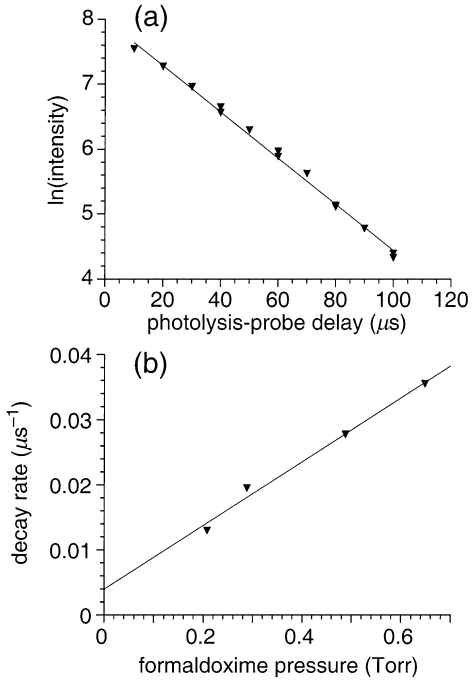

Figure 4. (a) Semilogarthmic plot of the OH $A - X$ (1,0) LIF signal vs delay time. The pressure of formaldoxime was 0.58 Torr. (b) Plot of the first-order decay rate constant vs formaldoxime pressure. The slope of the plot is the bimolecular rate constant of the OH + CH_2-NOH reaction.

at short photolysis-probe delays is presented there. The decrease of the magnitude of the OH signal is due to the fast reaction of OH radical with the formaldoxime precursor. Since knowledge of this rate constant is of practical importance when comparison of OH and H_2CN signals is made, the rate constant of this reaction was determined. This measurement is described in the next section.

3.2. Reaction of OH with CH_2NOH. To measure the rate constant of the OH + CH_2NOH reaction, the laser-induced OH $A - X$ fluorescence signal, which is proportional to the OH radical concentration, was monitored while the delay between the photolysis and detection lasers was varied. The LIF signal was excited on one of the rotational lines [$R_1(3/2)$] of the $A - X$ (1,0) band and monitored by collecting all fluorescence in the $A - X$ (1,1) band. The photolysis laser energy was reduced to ~0.5 mJ to avoid possible problems associated with radical recombination reactions. A typical plot of the logarithm of the OH LIF signal vs the delay time is shown in Figure 4a. This plot is linear over three decay lifetimes, consistent with the assumed first-order kinetics model. The bimolecular rate constant for the OH + CH_2NOH reaction was calculated from the plot of the first-order decay rate constant vs CH_2NOH pressure, shown in Figure 4b, and this rate constant is determined to be $(1.5 \pm 0.4) \times 10^{-12}$ cm^3 molecule^{-1} s^{-1}. This value is significantly different from that determined by Horne and Norrish[15] [0.6×10^{-12} cm^3 molecule^{-1} s^{-1} ($\pm$50%)]. A small nonzero intercept on the plot in Figure 4b of the first-order rate constant vs pressure is likely due to the diffusion of OH out of the photolysis volume. This removal process should not interfere with the bimolecular rate constant measurement since it is significantly slower than removal due to the chemical reaction. Below, other possible sources of systematic errors in our measurement are addressed.

The OH concentration in this experiment can be estimated from the precursor absorption cross section at 193 nm and photon density of the photolysis laser. For this experiment, [OH]

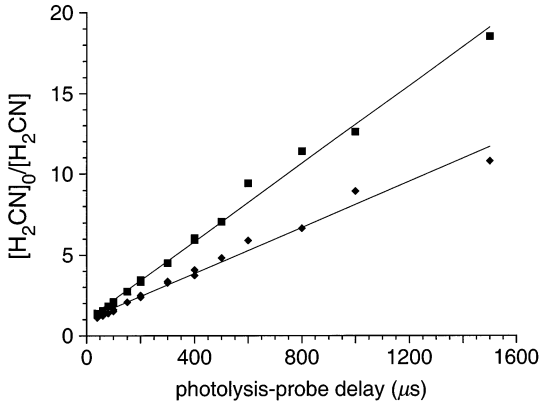

Figure 5. Plot of the $[H_2CN]_0/[H_2CN]$ concentration ratio vs delay time. The partial pressures of formaldoxime and Ar were ~300 mTorr and 5 Torr, respectively. The slope of the fitted lines are proportional to the $[H_2CN]_0$, which was varied by changing the photolysis laser energy. Diamonds and squares correspond to photolysis laser energies of 20 mJ and 40 mJ, respectively. The ratio of the slopes is approximately equal to the ratio of the photolysis laser energies.

is estimated to be $< 2 \times 10^{13}$ cm^{-3}. The room-temperature, low-pressure bimolecular recombination rate constant,[32] $k(OH + OH) = 1.9 \times 10^{-12}$ cm^3 molecule^{-1} s^{-1}, is too small for the OH + OH reaction to compete with the OH + CH_2NOH reaction. The rate constant for OH + H_2CN reaction, estimated below in Section 3.5 to be 6×10^{-12} cm^3 molecule^{-1} s^{-1}, is also too small for this reaction to contribute significantly to the removal rate of [OH]. Thus, OH + OH and OH + H_2CN recombination cannot compete with the OH + CH_2NOH reaction under the conditions of this experiment.

Since the synthesis[29] of formaldoxime is carried out in aqueous solution, we were concerned that the discrepancy between our value for the rate constant of the OH + CH_2NOH and that of Horne and Norrish[15] could be due to the presence of water. The rate constant was measured with different samples, which had been pumped on for various lengths of time. The same rate constant was obtained with all samples of formaldoxime and indicates that the water content is not an issue. We believe that our measurement is more reliable than that of Horne and Norrish[15] since it is more direct.

3.3. Self-Recombination of the H_2CN Radical. An attempt was made to study reactions of H_2CN with stable molecular reagents. However, in all of the experiments, the time dependence of the H_2CN signal was consistent with the fact that self-recombination of H_2CN rather than reaction of H_2CN with the buffer gas was the main process that decreased the H_2CN concentration. If one defines the radical−radical recombination rate constant as k_{self} through the following equation:

$$d[H_2CN]/dt = -2k_{self}[H_2CN]^2 \quad (1)$$

then the time dependence of the H_2CN concentration will be

$$[H_2CN]_0/[H_2CN] = 1 + 2k_{self}[H_2CN]_0 t \quad (2)$$

The initial concentration $[H_2CN]_0$ and the time-dependent concentration $[H_2CN]$ can be computed from the differences in the CRD decay lifetimes with the photolysis laser on vs off at various photolysis-probe delays t.

Figure 5 presents plots of the concentration ratio $[H_2CN]_0/[H_2CN]$ as a function of the photolysis-probe delay for two different energies of the photolysis laser. We see that for both photolysis laser energies, the concentration ratio is linearly proportional to the photolysis-probe delay, in accord with eq 2. It should also be noted that the range of photolysis-probe delays is much greater than the CRD decay lifetime, so that effects of the time scale of the CRD concentration measurement[33] can be ignored in the kinetic analysis.

We also see from Figure 5 that the slope appears to scale with the photolysis laser energy. This follows from eq 2 since the initial H_2CN concentration $[H_2CN]_0$ should be proportional to the photon density of the photolysis laser, if the photolysis volume is not changed and the fractional dissociation is not high. The measurement of the dependence of the slope of the $[H_2CN]_0/[H_2CN]$ concentration ratio upon the photolysis laser photon density can be used to test whether removal of is due to self-recombination or other processes contribute to the reduction of the H_2CN concentration. In all experiments where the fraction of dissociation was small (<4%), the slopes of plots of the concentration ratio vs the photolysis-probe delay were found to be linearly dependent on the photolysis laser photon density to within experimental uncertainty. This confirms that recombination was the main loss mechanism for H_2CN.

The slope of plots of the concentration ratio $[H_2CN]_0/[H_2CN]$ equal $2k_{self}[H_2CN]_0$ when recombination is the dominant loss mechanism for H_2CN. The initial concentration of H_2CN can be computed from the CRD signal at short delays and the absorption cross section for H_2CN at 285 nm, whose determination is reported in the next section. In calculating $[H_2CN]_0$, we took into account the fact that the length of the photolysis volume along the axis of the resonant cavity was shorter than the cavity length. From experimental data such as those plotted in Figure 5, the value $k_{self} = (7.7 \pm 2.5) \times 10^{-12}$ cm^3 molecule^{-1} s^{-1} was determined. The value for the absorption cross section, $\sigma(285\text{ nm}) = 1.1 \times 10^{-18}$ cm^2, reported below in the next section, was employed. Our derived value for the recombination rate constant compares well with the value $k_{self} = 5.8 \times 10^{-12}$ cm^3 molecule^{-1} s^{-1} determined by Horne and Norrish.[15]

We have attempted to observe the reactions of H_2CN with stable molecules. Our choice of two of the reagents to study [O_2, C_2H_4] was dictated by the availability of an exothermic hydrogen abstraction pathway, i.e.

$$H_2CN + O_2 \rightarrow HCN + HO_2 \quad (3a)$$

$$H_2CN + C_2H_4 \rightarrow HCN + C_2H_5 \quad (3b)$$

Reactions with several other reagents [CO, CH_4, H_2] were also studied. For these experiments the typical pressure of the reagent was 100 Torr. While reaction with none of these stable molecular reagents was observed, we estimate from the reagent pressure and time dependence of the H_2CN concentration upper limits of the rate constants for these reactions to be $< 1 \times 10^{-15}$ cm^3 molecule^{-1} s^{-1}.

3.4. Absorption Strength of the H_2CN Transition. One can calculate the absorption cross section of H_2CN from an estimated H_2CN concentration and the observed H_2CN absorption. The H_2CN concentration can be estimated from the known absorption cross section of the precursor at the photolysis wavelength, the photolysis laser photon density, and H_2CN quantum yield from formaldoxime photolysis. It was assumed that the H_2CN quantum yield from photolysis was equal to unity. For calculation purposes, the absorption cross section of formaldoxime at 193 nm, $\sigma(193\text{ nm}) = 1.5 \times 10^{-18}$ cm^2 from ref 15 was used. In a typical experiment, ~4% of the precursor was estimated to be photodissociated in each photolysis laser shot. The CRD signal at zero delay between the photolysis and detection laser pulses was obtained by measuring the H_2CN CRD signal at long delay times, $t > 20$ μs, when relaxation of H_2CN was complete

and then extrapolating to $t = 0$ μs using the plot of $(1/\tau - 1/\tau_0)^{-1}$ vs time. From this method, the absorption cross section of H_2CN at 285 nm was determined to be 1.1×10^{-18} cm^2, in a good agreement with the results by Horne and Norrish[11] and measurements based on comparison of OH and H_2CN signals, described below. This value of the absorption cross section was employed in the previous section in the determination of the H_2CN recombination rate constant.

It is also possible to calculate the H_2CN absorption strength by comparison of the OH and H_2CN signals, since both the H_2CN transitions and the OH $A - X$ (1,0) band lie in the same wavelength region. The oscillator strength of the OH $A - X$ (1,0) band ($f = 2.8 \times 10^{-4}$) is well established.[34] Since the ratio of OH and H_2CN concentrations can be determined, comparison of the OH and H_2CN signals should yield absorption strength of H_2CN. Dagdigian et al.[18] measured the nascent internal state distribution of the OH radical and concluded that OH radical has little vibrational excitation and all of the population is in the ground vibrational state, $v'' = 0$. It was assumed that vibrational relaxation of H_2CN was complete, and all of the population was in the ground vibrational level. It was also assumed that the quantum yields of H_2CN and of OH were both equal (to unity).

Corrections for the loss of OH and H_2CN due to the chemical reactions were made as follows. The main loss mechanism of OH was assumed to be the reaction of OH with formaldoxime, while the main loss mechanism of H_2CN was assumed to be self-recombination. As described above, the H_2CN signal at $t = 0$ μs can be obtained from the intercept of $(1/\tau - 1/\tau_0)^{-1}$ vs time plot.

To measure the OH absorption quantitatively using the CRDS technique, the laser bandwidth has to be much smaller than Doppler width of the OH rotational lines. With the intracavity Etalon installed in the detection dye laser, the nominal laser bandwidth is 0.08 cm^{-1}, compared to the Doppler width of the OH $A - X$ (1,0) rotational lines [0.11 cm^{-1}]. It is still possible to measure the absorption coefficient integrated over wavelength, provided that absorption losses due to OH are much smaller than the empty cavity losses and only a small initial part of the CRD signal is used to measure decay time. For details, the paper of Zalicki and Zare,[35] or papers mentioned in a review by Meijer and co-workers,[20] can be consulted. Typically, the ratio of losses due to OH absorption to the empty cavity losses was <0.2 and the time interval $0 < t < \sim 0.5\tau_0$, where τ_0 is the empty cavity decay time, was used to calculate decay time. For the other measurements, the time interval $0 < t < \sim 2.5\tau_0$ was used to calculate decay time.

Since it was difficult to record the complete spectrum of the OH $A - X$ (1,0) band because of the low data collection rate, only a small portion of the (1,0) band was recorded. Specifically, six rotational lines [$R_1(3/2)$, $R_1(5/2)$, $R_1(7/2)$, $Q_{21}(3/2)$, $Q_{21}(5/2)$, and $Q_{21}(7/2)$] were used to determine the OH concentration. One important advantage of using these six lines is that their wavelengths are close to 280.8 nm, i.e., the maximum of one of the H_2CN bands, which enables a more accurate measurement of the H_2CN absorption. It also should be noted that the lower states for these six rotational lines represent ~54% of the OH population.

As mentioned by Dagdigian et al.,[18] the nascent OH internal state distribution from 193 nm CH_2NOH photolysis was somewhat hotter than a room-temperature Boltzmann distribution. For measurement of the OH signal, the delay between the photolysis and detection lasers was chosen long enough to ensure that collisions with the buffer gas produced a room-temperature rotational distribution. As diagnostics, LIF spectra of OH were recorded for different delays between the photolysis and detection lasers. It was found that for conditions $p \times t > 20$ Torr μs in Ar the OH rotational state distribution was close to its room-temperature Boltzmann distribution.

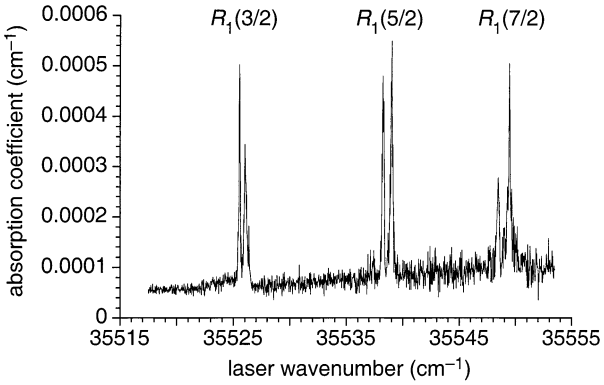

Figure 6. High-resolution (laser bandwidth 0.08 cm^{-1}) CRD spectrum of OH and H_2CN collected at 3 μs delay between the photolysis and detection laser pulses in the presence of 300 mTorr formaldoxime and 5 Torr Ar. The $R_1(J)$ main and $Q_{21}(J)$ satellite lines of the OH $A - X$ (1,0) band are marked. The unstructured continuum is due to absorption by H_2CN.

A high-resolution OH CRD spectrum is shown in Figure 6. For this spectrum, the OH concentration was calculated to be 3.9×10^{14} cm^{-3}. For this calculation, the Einstein B coefficients from the LIFBASE program[36] for rotational lines of the OH $A - X$ (1,0) band was used. The calculated OH concentration corresponds to a 4% precursor photodissociation on each shot, close to the number calculated using the formaldoxime absorption cross section at 193 nm and the photolysis laser photon density. From the OH concentration, the H_2CN absorption oscillator strength was computed to be $f = 4.5 \times 10^{-4}$. The oscillator strength value is in good agreement with the value, $f = (4 \pm 2) \times 10^{-4}$, reported by Ogilvie and Horne.[10]

3.5. Rate Constant for the OH + H_2CN Reaction. To measure the OH + H_2CN rate constant, it is necessary to dissociate a significant fraction of the precursor so that the OH + H_2CN reaction can compete with the OH + H_2CNOH reaction. This was done by removing one of the cylindrical lenses, thereby changing the photolysis laser beam dimensions to 24×2 mm^2. In addition, the photolysis laser energy inside the CRDS apparatus was increased. Based on the known absorption cross section of formaldoxime[15] and photolysis laser energy, it was estimated that a maximum of ~35% dissociation could be achieved. The variation of the H_2CN concentration perpendicular to the axis of the resonant cavity was small, because of the small diameter (0.05 cm) of the probe laser beam.

Figure 7 shows experimental measurements of the OH and H_2CN concentrations (points), along with the results of kinetic simulations (solid curves) used to derive the OH + H_2CN rate constant. One of the curves represents the time dependence of the OH concentration at low photolysis laser energies and was recorded to compute the concentration of the formaldoxime precursor from the measured OH decay rate, using our derived value for the OH + H_2CNOH rate constant. It should be noted that under the conditions of this experiment the formaldoxime concentration could not be directly measured since a large excess of Ar was added to promote rapid collisional relaxation of the OH and H_2CN radicals. For low photolysis laser energies, radical−radical reactions involving OH can be neglected, and the decay of the OH concentration can be ascribed to the OH

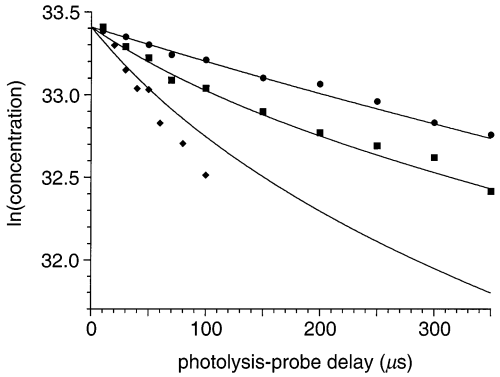

Figure 7. Experimental and simulated time dependence of OH and H_2CN concentrations at high and low excimer laser energies. The formaldoxime pressure was 0.03 Torr, and the buffer gas pressure (Ar) was 200 Torr. The solid circles are measured OH concentrations at low photolysis laser energy, while the squares and diamonds are OH and H_2CN concentrations, respectively, at high photolysis laser energy. The solid curves are concentrations obtained from kinetic simulations described in the text. In the plot, the initial concentration of OH at low photolysis laser energy was made the same as the initial concentration of OH at high photolysis laser energy for ease of comparison.

+ H_2CNOH reaction. From the first-order rate constant of the OH concentration decay and our measured value of k(OH + H_2CNOH) reported above, the formaldoxime precursor concentration in this particular experiment was calculated to be 0.033 Torr.

The other two sets of points in Figure 7 represent the time dependence of the OH and H_2CN concentrations at high photolysis laser energy, but otherwise under the same conditions. From the CRDS signal for H_2CN, the absolute concentration of H_2CN was calculated to be 0.010 Torr. The ratio of the derived H_2CNOH precursor and H_2CN radical concentrations implies a 30% dissociation of the precursor, which is consistent with the estimate made using the measured photolysis laser energy and the known formaldoxime absorption cross section. The good agreement of the fractional dissociation estimated by two different methods implies that multiphoton effects due to the photolysis laser can be neglected.

The initial slopes of the OH concentration curves at low and high photolysis laser energies differ significantly, with the removal rate of OH being larger at high photolysis laser energy. This suggests that the rate constant of the OH + H_2CN reaction is larger than the rate constant of the OH + H_2CNOH reaction. To derive a numerical value of k(OH + H_2CN), a kinetic simulation was performed with the following set of reactions:

$$\mathrm{OH} + \mathrm{H_2CN} \rightarrow \text{products, } k \text{ to be determined}$$

$$\mathrm{OH} + \mathrm{OH} \rightarrow \mathrm{H_2O} + \mathrm{O}, \qquad k = 1.9 \times 10^{-12}\ \mathrm{cm^3\ molecule^{-1}\ s^{-1}}$$

$$\mathrm{OH} + \mathrm{H_2CNOH} \rightarrow \text{products}, \qquad k = 1.5 \times 10^{-12}\ \mathrm{cm^3\ molecule^{-1}\ s^{-1}}$$

$$\mathrm{H_2CN} + \mathrm{H_2CN} \rightarrow \text{products}, \qquad k = 7.7 \times 10^{-12}\ \mathrm{cm^3\ molecule^{-1}\ s^{-1}}$$

$$\mathrm{H_2CN} + \mathrm{H_2CNOH} \rightarrow \text{products}, \qquad k = 0 \times 10^{-12}\ \mathrm{cm^3\ molecule^{-1}\ s^{-1}}$$

This model does not take into consideration secondary reactions. Hence, only the measured concentrations at short photolysis-probe delays, corresponding to a small extent of reaction, were considered. In the kinetic simulations, the rate constant for the OH + H_2CN reaction was varied to fit the initial slope of the OH concentration, while keeping the rate constants of the other reactions fixed. The best fit to the experimental data was achieved for k(OH + H_2CN) = 6×10^{-12} cm^3 $molecule^{-1}$ s^{-1}. We estimate that this rate constant was determined to an accuracy of 30−50%, given the uncertainties in the other rate constants and the H_2CN absorption cross section. We did not attempt to vary the rate constants of the other reactions since the initial slope is determined mainly by the rate constants of the OH + H_2CN and H_2CNOH reactions, and we have directly measured the rate constant of the latter reaction (see Section 3.2).

One can note a significant discrepancy between experimental and simulated time dependence of the H_2CN concentration, with the computed falloff in concentration being less than the observed falloff. This difference cannot be minimized by varying the k(OH + H_2CN) rate constant. However, a good-quality fit to the experimental data can be achieved if one varies k(OH + H_2CN), k(H_2CN + H_2CN), and σ(285 nm) within their uncertainty limits. Thus, the discrepancy is likely to be due to the limited precision in the measurement of the other rate constants and the H_2CN absorption cross section.

One of the possible complications in this experiment is local heating of the sample due to the large amount of photolysis laser energy absorbed by the sample. In this particular experiment, 200 Torr of buffer gas (Ar) and 0.03 Torr of the formaldoxime vapor was used. For the experimentally determined 30% dissociation, this translates into a 2.5 K increase in the sample temperature on a single photolysis laser shot. It is also worth mentioning that the recorded LIF spectrum of OH was consistent, within experimental uncertainty, with a room-temperature rotational state distribution. Thus, the actual temperature of the sample was very close to the room temperature.

The other possible complication could be the pressure dependence of the H_2CN recombination rate constant. Horne and Norrish[11] note that in their pressure range (100−500 Torr), the H_2CN recombination was pressure independent. Since the pressure range in this work was similar to the one employed by Horne and Norrish, it was assumed that the rate constant k(H_2CN + H_2CN) determined in this work is in the high-pressure limit. For the OH + H_2CN rate constant, the measurements were done at two pressures, 120 and 200 Torr of Ar, and the derived value for k(OH + H_2CN) was essentially the same at these two pressures. Thus, it was assumed that k(OH + H_2CN) determined in this work is in the high-pressure limit.

4. Discussion

In this work, we have employed CRDS to investigate the room-temperature reaction kinetics of the H_2CN radical, which was prepared by 193 nm photolysis of formaldoxime. We have obtained a rate constant for the H_2CN recombination rate constant, in good agreement with an earlier measurement by flash photolysis.[11] Only upper limits to the room-temperature rate constants for reaction of H_2CN with several stable molecules, including oxygen and ethylene, could be obtained. By increasing the energy density of the photolysis laser, thereby photolyzing a significant fraction of fomaldoxime, it was possible to study the fraction between the OH and H_2CN radicals. In this way, a room-temperature rate constant of 6×10^{-12} cm^3 $molecule^{-1}$ s^{-1} was estimated for this reaction. This rate constant is actually significantly less than the rate constants determined by Nesbitt et al.[19] for the reactions of H_2CN with

N and H atoms: $k(N + H_2CN) = (4.4 \pm 1.4) \times 10^{-11}$ cm^3 molecule^{-1} s^{-1} and $k(H + H_2CN) \geq 7 \times 10^{-11}$ cm^3 molecule^{-1} s^{-1}.

It is also interesting to compare the rate constants for reactions of H_2CN with those for corresponding reactions of the isoelectronic HCO radical.[37−39] The room-temperature rate constant for the HCO + O_2 reaction [$(5.9 \pm 0.5) \times 10^{-12}$ cm^3 molecule^{-1} s^{-1} (ref 38)] is significantly larger than that for the corresponding H_2CN reaction. By contrast, the room-temperature rate constant for the reaction of ethylene with HCO [1.5×10^{-17} cm^3 molecule^{-1} s^{-1} (ref 37)] is quite small, as in the case of the corresponding reaction involving H_2CN. For the HCO reaction, the activation energy is 5.5 kcal mol^{-1}, and reactions of other alkenes have similar rate constants and activation energies. Similar to the H + H_2CN reaction, the H + HCO reaction has a very large room-temperature rate constant [$(1.13 \pm 0.33) \times 10^{-10}$ cm^3 molecule^{-1} s^{-1} (ref 39)].

The OH + H_2CN reaction likely proceeds through a hydrogen abstraction channel:

$$OH + H_2CN \rightarrow HCN + H_2O \qquad (4)$$

Our derived room-temperature rate constant for this reaction is quite similar to the reported[40] rate constant [$(7.75 \pm 1.24) \times 10^{-12}$ cm^3 molecule^{-1} s^{-1}] for the OH + H_2CO reaction. This reaction was found[40] to proceed predominantly by hydrogen atom abstraction, as in eq 4.

In the present study, study of the reactions of H_2CN with stable molecules was limited by the low room-temperature rate constants and the fast H_2CN self-recombination rate. This does not preclude the future investigation of these reactions by CRDS. An obvious solution is to use smaller H_2CN concentrations and to study faster reactions. By using higher reflectivity mirrors and studying reactions at higher temperatures, where reaction rate constants are larger, important additional information about the chemical reactions of H_2CN could be obtained.

Acknowledgment. This work was supported by the U.S. Army Research Office (ARO), under Grant DAAD19-02-1-0323. The excimer laser employed as the photolysis light source was acquired with funds from ARO Grant DAAD19-00-1-0022.

References and Notes

(1) Marston, G.; Steif, L. J. *Res. Chem. Intermed.* **1989**, *12*, 161.
(2) Morgan, C. U.; Beyer, R. A. *Combust. Flame* **1979**, *36*, 99.
(3) Alexander, M. H.; Dagdigian, P. J.; Jacox, M. E.; Kolb, C. E.; Melius, C. F.; Rabitz, H.; Smooke, M. D.; Tsang, W. *Prog. Energy Combust. Sci.* **1991**, *17*, 263.
(4) Adams, G. F.; Shaw, R. W., Jr. *Annu. Rev. Phys. Chem.* **1992**, *43*, 311.
(5) Marston, G.; Nesbitt, F. L.; Nava, D. F.; Payne, W. A.; Steif, L. J. *J. Phys. Chem.* **1989**, *93*, 5769.
(6) Marston, G.; Nesbitt, F. L.; Steif, L. J. *J. Chem. Phys.* **1989**, *91*, 3483.
(7) Miller, J. A.; Melius, C. F.; Glarborg, P. *Int. J. Chem. Kinet.* **1998**, *30*, 223.
(8) Lebonnois, S.; Toublanc, D.; Houdin, F.; Rannou, P. *Icarus* **2001**, *152*, 384.
(9) Cochran, E. L.; Adrian, F. J.; Bowers, V. A. *J. Chem. Phys.* **1962**, *36*, 1938.
(10) Ogilvie, J. F.; Horne, D. G. *J. Chem. Phys.* **1968**, *48*, 2248.
(11) Horne, D. G.; Norrish, R. G. W. *Proc. R. Soc. London Ser. A* **1970**, *315*, 1970.
(12) Jacox, M. E.; Milligan, D. E. *J. Mol. Spectrosc.* **1975**, *56*, 333.
(13) Nesbitt, F. L.; Marston, G.; Steif, L. J.; Wickramaaritchi, M. A.; Tao, W.; Klemm, R. B. *J. Phys. Chem.* **1991**, *95*, 7613.
(14) Bernard, E. J.; Strazisar, B. R.; Davis, H. F. *Chem. Phys. Lett.* **1999**, *313*, 461.
(15) Horne, D. G.; Norrish, R. G. W. *Proc. R. Soc. London Ser. A* **1970**, *315*, 287.
(16) Felder, P.; Harrison, J. A.; Huber, J. R. *J. Phys. Chem.* **1991**, *95*, 1945.
(17) Jacox, M. E. *J. Phys. Chem.* **1987**, *91*, 6595.
(18) Dagdigian, P. J.; Anderson, W. R.; Sausa, R. C.; Miziolek, A. W. *J. Phys. Chem.* **1989**, *93*, 6059.
(19) Nesbitt, F. L.; Marston, G.; Steif, L. J. *J. Phys. Chem.* **1990**, *94*, 4946.
(20) Berden, G.; Peeters, R.; Meijer, G. *Int. Rev. Phys. Chem.* **2000**, *19*, 565.
(21) Wheeler, M. D.; Newman, S. M.; Orr-Ewing, A. J.; Ashfold, M. N. R. *J. Chem. Soc., Faraday Trans.* **1998**, *94*, 337.
(22) Booth, J. P.; Cunge, G.; Biennier, L.; Romanini, D.; Kachanov, A. *Chem. Phys. Lett.* **2000**, *317*, 631.
(23) Luque, J.; Jeffries, J. B.; Smith, G. P.; Crosley, D. R.; Scherer, J. J. *Combust. Flame* **2001**, *126*, 1725.
(24) Adams, G. F.; Yarkony, D. R.; Bartlett, R. J.; Purvis, G. D. *Int. J. Quantum Chem.* **1983**, *23*, 437.
(25) So, S. P. *Chem. Phys. Lett.* **1981**, *82*, 370.
(26) Brinkmann, N. R.; Wesolowski, S. S.; Schaefer, H. F. *J. Chem. Phys.* **2001**, *114*, 3055.
(27) Bair, R. A.; Dunning, T. H. *J. Chem. Phys.* **1985**, *82*, 2280.
(28) ter Horst, M. A.; Schatz, G. C.; Harding, L. B. *J. Chem. Phys.* **1996**, *105*, 559.
(29) Scholl, R. *Berichte* **1891**, *24*, 573.
(30) Dieke, G. H.; Crosswhite, H. M. *J. Quant. Spectrosc. Radiat. Transfer* **1962**, *2*, 97.
(31) Herzberg, G. *Molecular Spectra and Molecular Structure III. Electronic Spectra and Electronic Structure of Polyatomic Molecules*; D. Van Nostrand: Princeton, 1967.
(32) Forster, R.; Frost, M.; Fulle, D.; Hamann, H. F.; Hippler, H.; Schlepegrell, A.; Troe, J. *J. Chem. Phys.* **1995**, *103*, 2949.
(33) Brown, S. S.; Ravishankara, A. R.; Stark, H. *J. Phys. Chem. A* **2000**, *104*, 7044.
(34) Luque, J.; Crosley, D. R. *J. Chem. Phys.* **1998**, *109*, 439.
(35) Zalicki, P.; Zare, R. N. *J. Chem. Phys.* **1995**, *102*, 2708.
(36) LIFBASE <http://www.sri.com/psd/lifbase/> is a freeware program and database written by J. Luque (SRI International) for the simulation of the spectra of diatomic molecules.
(37) Lesclaux, R.; Roussel, R.; Veyret, B.; Pouchan, C. *J. Am. Chem. Soc.* **1986**, *108*, 3872.
(38) Nonimiya, Y.; Goto, M.; Hashimoto, S.; Kagawa, Y.; Yoshizawa, K.; Kawasaki, M.; Wallington, T. J.; Hurley, M. D. *J. Phys. Chem. A* **2000**, *104*, 7556.
(39) Ziemer, H.; Dóbé, S.; Wagner, H. G.; Olzmann, M.; Viskolcz, B.; Temps, F. *Ber. Bunsen-Ges. Phys. Chem.* **1998**, *102*, 897.
(40) Yetter, R. A.; Rabitz, H.; Dryer, F. L.; Maki, R. G.; Klemm, R. B. *J. Chem. Phys.* **1989**, *91*, 4088.